

Interstellar Plasma Turbulence Spectrum Toward the Pulsars PSR B0809+74 and B0950+08

T. V. Smirnova¹ and V. I. Shishov¹

¹*Pushchino Radio Astronomy Observatory, Astro Space Center of the Lebedev Institute of Physics, Russian Academy of Sciences, Pushchino, Moscow oblast', 142290 Russia*

Interstellar scintillations of pulsars PSR B0809+74 and B0950+08 have been studied using observations at low frequencies (41, 62, 89, and 112 MHz). Characteristic temporal and frequency scales of diffractive scintillations at these frequencies have been determined. The comprehensive analysis of the frequency and temporal structure functions reduced to the same frequency has shown that the spectrum of interstellar plasma inhomogeneities toward both pulsars is described by a power law. The exponent of the spectrum of fluctuations of interstellar plasma inhomogeneities toward PSR B0950+08 ($n = 3.00 \pm 0.05$) appreciably differs from the Kolmogorov exponent. Toward PSR B0809+74 the spectrum is a power law with an exponent $n = 3.7 \pm 0.1$. A strong angular refraction has been detected toward PSR B0950+08. The distribution of inhomogeneities along the line of sight has been analyzed; it has been shown that the scintillations of PSR B0950+08 take place on a turbulent layer with enhanced electron density, which is localized at approximately 10 pc from the observer. For PSR B0809+74 the distribution of inhomogeneities is quasi-uniform. Mean-square fluctuations of electron density on inhomogeneities with a characteristic scale $\rho_0 = 10^7$ m toward four pulsars have been estimated. On this scale the local turbulence level in the 10-pc layer is 20 times higher than in an extended region responsible for the scintillations of PSR B0809+74.

1. INTRODUCTION

Pulsars represent a good tool for the study of interstellar plasma (ISP), because they possess very small angular sizes and intense emission. The investigation of their intensity fluctuations in the frequency–time domain allows us to study the ISP spectrum in various directions of our Galaxy. As was shown in [1, 2], the observational data on pulsar scintillations are statistically well described by a power-law spectrum of inhomogeneities with an exponent $n = 3.67$ (i.e., by the Kolmogorov spectrum) in a very broad range of spatial scales ρ . However, a scatter in the values of the spectrum exponent n is observed for the same value of ρ for different sources; this testifies that in local directions of the Galaxy the spectrum can differ from the Kolmogorov spectrum. The application of a new method for the study of ISP using a comprehensive analysis of a structure function obtained from multifrequency observations of pulsar scintillations has revealed a difference of the spectrum from Kolmogorov's for PSR B0329+54, B0437–47, and B1642–03 [3–5]. The purpose of this paper was a study of the ISP spectrum toward nearby and powerful at meter wavelengths pulsars PSR B0809+74 and B0950+08. The distances to these pulsars and their velocities are known from parallax measurements [6]: $R = 433$ pc, $V = 102$ km/s and $R = 262$ pc, $V = 36.6$ km/s for PSR B0809+74 and B0950+08 respectively. Since they are the nearest pulsars, the analysis of their scintillations allows us to study the region of interstellar plasma nearest to the Sun.

The obtained earlier observational data demonstrate the presence of three components of interstel-

lar turbulent plasma in the solar neighborhood at distances of the order of 1 kpc and less. The first component is turbulent plasma with a statistically quasi-uniform distribution in the space between spiral arms (component A in the classification of [7, 8]). The second component represents a cavern with a depleted electron density ($n_e \cong 0.005$ cm⁻³) in the solar neighborhood with a scale of about 200–300 pc perpendicularly to the Galactic plane and 50–100 pc in the Galactic plane. This cavern has been detected in X-ray observations [9]. The presence of a cavern with a lowered turbulence level on a scale of the order of 100 pc has been revealed also by the analysis of scintillations of pulsars with dispersion measures from 3 to 35 pc cm⁻³ [10]. The third component corresponds to a layer with an enhanced turbulence level at a distance of about 10 pc from the Sun. This layer has been detected in observations of interstellar scintillations of quasars in the centimeter waveband [11, 12]. In [5] this layer was classified as component C. In [5] it was also shown that the pulsar PSR J0437–4715 scintillates on inhomogeneities of layer C.

2. OBSERVATIONS AND DATA PREPROCESSING

The observations of PSR B0809+74 and B0950+08 were carried out on the BSA and DKR-1000 radio telescopes of the Pushchino Radio Astronomy Observatory (Astro Space Center, Lebedev Institute of Physics, Russian Academy of Sciences) at frequencies 41, 62.43, 88.57 MHz (DKR-1000), and 111.87 MHz (BSA) in December

Table 1. Parameters of the observations

Parameter	f , MHz			
	41	62.43	88.57	111.87
PSR B0809+74				
Δt , ms	5.12; 2.56	5.15	5.38	2.56
N_{ch}	128; 64	96	96	128
Δf , kHz	1.25; 20	20	20	20
T , s	51.68	51.68	38.76	19.38
PSR B0950+08				
Δt , ms	5.12; 2.56	2.56	2.56	2.56
N_{ch}	64	96	128	128
Δf , kHz	1.25; 20	20	20	20
T , s	20.24	15.18	20.24	5.06

2001 – January 2004. As the interference situation at low frequencies was complex, we have used for the analysis only those records where interference was small. We received linearly polarized emission. Two multichannel receivers were used: a 128-channel receiver with a channel bandwidth $\Delta f = 20$ kHz at frequencies 88.57, 62.43, and 111.87 MHz as well as a 128-channel receiver with a channel bandwidth $\Delta f = 1.25$ kHz at a frequency of 41 MHz. The time of observations on BSA (frequency 111.87 MHz) in each session was 12 and 3.3 min for PSR B0809+74 and B0950+08 respectively. At low frequencies it was 35.5 min for PSR B0809+74 and 15.63 min for PSR B0950+08. Table 1 lists the time and frequency resolution (Δt and Δf) and the used number of channels (N_{ch}) at each frequency. Individual pulses of the pulsars were recorded on the computer disk in all channels with a period synchronized with the precomputed topocentric pulse arrival time. Then the signal in all channels was shifted in accordance with the dispersion shift at the given frequency (reduction to the highest frequency channel); in channels affected by interference (if any) the signal was replaced by an average value found from the adjacent channels. The amplification in all channels was reduced to the same value by normalization, so that the noise dispersion in all channels were equal to its average value found from channels not affected by interference. At frequencies 41–89 MHz the record was performed in a window $1.8 P_1$ (P_1 is the pulsar period) and at 112 MHz in a window $0.9 P_1$. To improve the signal-to-noise ratio (S/N), we averaged individual pulses: from 15 pulses at 112 MHz to 40 pulses at low frequencies. The averaging time T for both pulsars at all frequencies is listed in Table 1.

3. CORRELATION ANALYSIS OF THE DATA

To analyze the intensity variations of the pulse radiation as a function of frequency (channel number)

within the bandwidth of the multichannel receiver, we formed spectra of individual pulses $I(f_k)$ by averaging the signal in a selected range of longitudes of the pulse and in a region outside the pulse, on the noise segment of the record (for the same number of longitudes) $I_N(f_k)$ for each channel. Here $f_k = f + (k-1)\Delta f$ is the frequency of the k th channel, and f is the frequency of observation. Then we subtracted the noise component $I_N(f_k)$ from $I(f_k)$, and the spectra of individual pulses thus obtained were analyzed with the purpose to get information in the frequency as well as in the time domains.

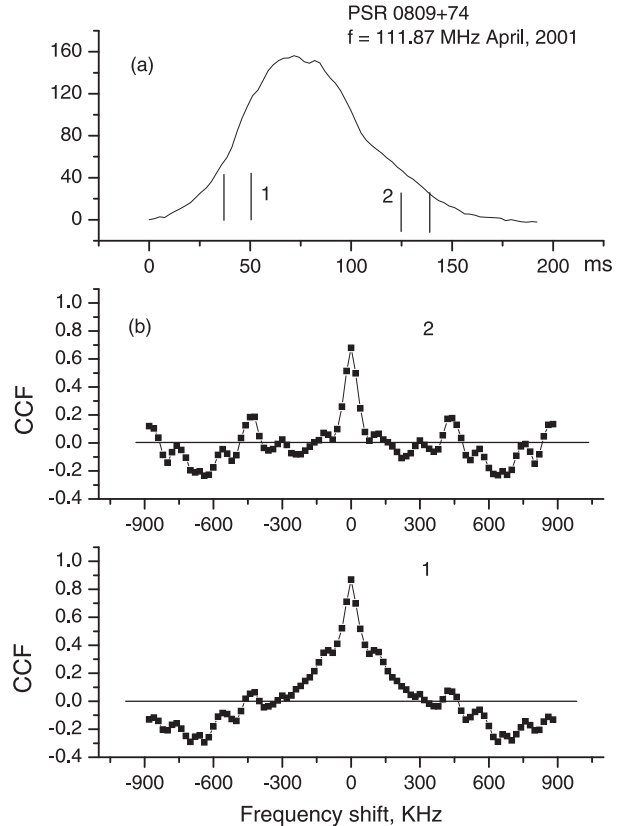


Figure 1. (a) Mean pulse profile of PSR B0809+74 at a frequency of 111.87 MHz as observed on April 6, 2001. Vertical axis: intensity in relative (computer) units; horizontal axis: time inside the pulse in milliseconds. Longitude ranges (interval 1 and interval 2) in which the pulse intensity was averaged are marked. (b) Mean normalized CCF between the spectra of adjacent pulses whose intensities were averaged in the above-mentioned longitude ranges: 1 (lower panel) and 2 (upper panel).

Characteristic frequency (f_{dif}) and temporal (t_{dif}) scales of scintillations were determined using the correlation analysis. We computed the mean cross-correlation function (CCF) between the spectra of adjacent, noiseless pulses averaged in the given range of longitudes of the pulse emission; CCF was normalized to the product of rms deviations $\sigma_1\sigma_2$. We con-

sidered a pulse as noiseless if its amplitude exceeded a level of $4\sigma_N$. The mean profile of the pulsar was derived by addition of all individual pulses in the given observational session. Since the pulse averaging time T (Table 1) was considerably shorter than the scintillation timescale, the decorrelation of the spectra of adjacent (averaged) pulses was insignificant; in return, we completely eliminated the uncorrelated component of noise. The frequency scale f_{dir} was determined as a frequency shift at which CCF decreased by a factor of two.

Since we receive linearly polarized emission, we must take into consideration the influence of polarization on its frequency–time structure. At low frequencies the degree of polarization for pulsars studied by us is high: about 60% for PSR B0809+74 [13] at the longitudes of the leading part of the mean profile and much lower in its trailing part; (70–80)% for PSR B0950+08 [14] throughout the profile. The rotation measure is $\text{RM} = -11.7 \text{ rad/m}^2$ for PSR B0809+74. The frequency of the Faraday rotation is

$$P_F \text{ [MHz]} = 17.475 f^3 / \text{RM}, \quad (1)$$

where f is the observational frequency in hundreds of megahertz. Accordingly, $P_F = 2140 \text{ kHz}$ at 112 MHz and $P_F = 59 \text{ kHz}$ at 41 MHz. The influence of polarization on the correlation analysis for PSR B0809+74 is shown in Fig. 1. Longitude ranges in which we averaged the intensity to obtain the spectra used in the calculation of the average CCF are shown. When averaging the leading part of the pulse (interval 1), a superposition of two structures—narrow-band (produced by propagation of the radiation in the interstellar plasma) and broadband (due to a much slower intensity variation with frequency as a result of the rotation of the polarization plane across the receiver bandwidth)—is visible. When averaging the trailing part (interval 2), the slow component is virtually absent; this confirms the small degree of polarization at these longitudes. In the frequency–time data analysis of PSR B0809+74 we have used the average over the longitudes of the trailing part of the mean profile.

For PSR B0950+08 the rotation measure is considerably smaller than for PSR B0809+74; however, in the literature its values appreciably differ: in the catalog of pulsars [15] $\text{RM} = (1.35 \pm 0.15) \text{ rad/m}^2$, in [14] $\text{RM} = (4\text{--}6) \text{ rad/m}^2$, and in [16] $\text{RM} = (-0.66 \pm 0.04) \text{ rad/m}^2$. Probably, authors [14] underestimated the contribution of the ionosphere to the obtained rotation measure. For $\text{RM} = 1 \text{ rad/m}^2$ the Faraday rotation frequency is $P_F = 20.4 \text{ MHz}$ at 112 MHz and $P_F = 1200 \text{ kHz}$ at 41 MHz. The influence of polarization on our observations at 41 MHz is shown in Fig. 2. The profile averaged over the session (Fig. 2a) is double-peaked with a separation between the components of 13 ms. Arrows shown

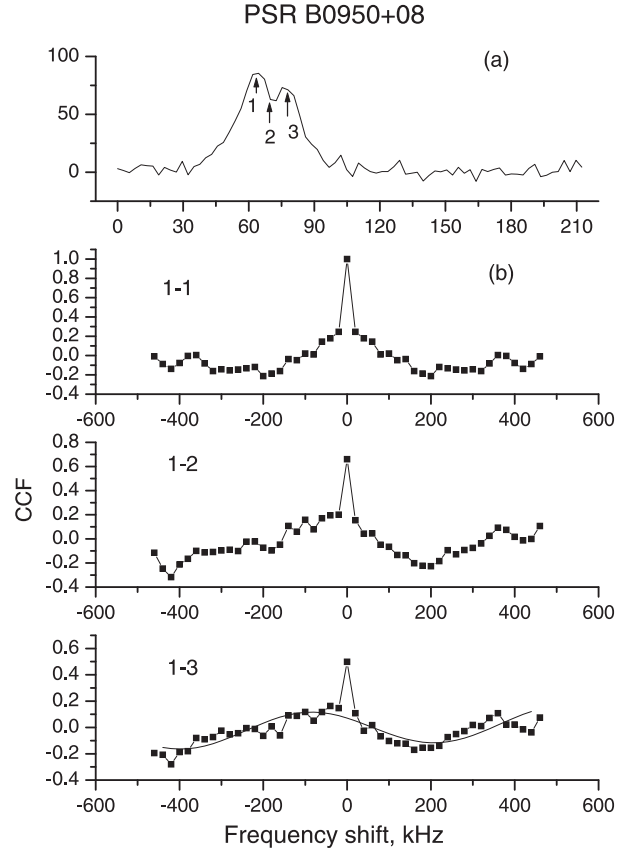


Figure 2. (a) Mean profile of PSR B0950+08 at a frequency of 41 MHz as observed on January 16, 2004. Vertical axis: intensity in relative (computer) units; horizontal axis: time inside the pulse in milliseconds. The time resolution is 2.56 ms, frequency resolution is 20 kHz. Arrows show longitudes at which the pulse intensity was selected in all channels for the calculation of the correlation functions. (b) Mean CCF between the pulse spectra taken at longitudes 1–1, 1–2, and 1–3. The curve in the lowermost graph is the fitted sine wave with a frequency of 600 kHz.

longitudes at which we selected pulse intensities over all channels to form the spectrum at the given longitude. Then we calculated mean normalized CCF between the spectra at longitudes 1–1 (autocorrelation function, ACF), 1–2, and 1–3 for all noiseless pulses. Figure 2b shows mean CCF between the spectra at the corresponding longitudes. In these observations we used the receiver with a channel bandwidth of 20 kHz. The narrow unresolved feature corresponding to the frequency scale of diffractive scintillations at 41 MHz has a maximum at the zero frequency shift, while the slow component is shifted to the left with an increase in the longitude offset of the spectra; this is due to the change in the position angle across the pulsar profile. Fitting a sine wave to the slow CCF component 1–3 yields the modulation frequency $P_F = (600 \pm 60) \text{ kHz}$, which corresponds

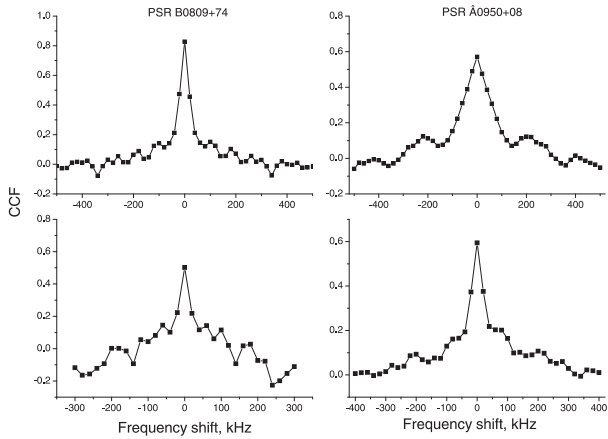


Figure 3. Mean normalized CCF for the spectra of adjacent pulses at 88.57 MHz (upper graphs) and 62.43 MHz (lower graphs) for PSR B0809+74 (left) and PSR B0950+08 (right).

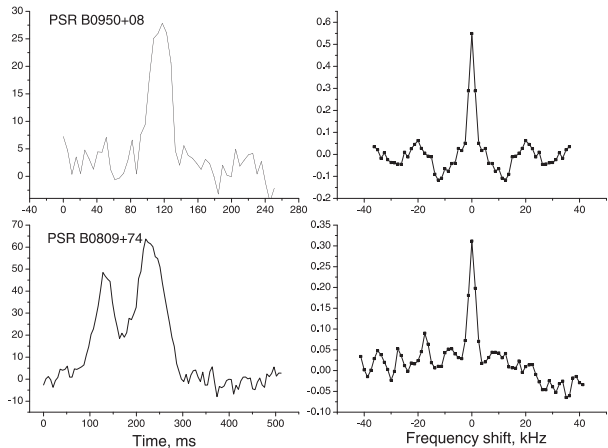


Figure 4. Mean profiles of PSR B0950+08 and PSR B0809+74 at 41 MHz as observed on December 25, 2003 (left) and mean normalized CCF between the spectra of adjacent pulses on this frequency (right). The time resolution is 5.12 ms, and the frequency resolution is 1.25 kHz. In the left graphs, the vertical axis plots the intensity in relative (computer) units, and the horizontal axis the time inside the pulse in milliseconds.

to $RM = (2 \pm 0.2) \text{ rad/m}^2$. The observations were carried out in the nighttime, and we suppose that the contribution of the ionosphere to this value was not more than 1 rad/m^2 . Consequently, RM toward PSR B0950+08 is about 1 rad/m^2 , and the effect of polarization on the frequency–time structure of the emission for this pulsar is considerably smaller than for PSR B0809+74. Therefore, for obtaining the spectra we used the average over all longitudes determined by the level of 0.25 of the mean profile maximum of the pulsar.

Figure 3 shows for both pulsars mean CCF between the spectra of adjacent pulses at 88.57 MHz

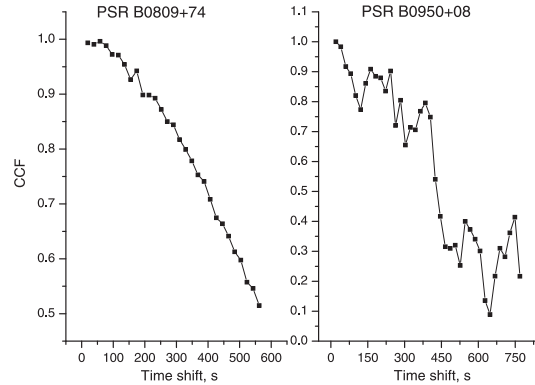


Figure 5. Mean normalized CCF for the spectra of pulses taken at appropriate time intervals (horizontal axis); left: for PSR B0809+74 at 111.87 MHz, right: for PSR B0950+08 at 88.57 MHz.

Table 2. Characteristic scales of diffractive scintillations

Parameter	f , MHz			
	41	62.43	88.57	111.87
PSR B0809+74				
f_{dif} , kHz	2 ± 0.6	7 ± 3	20 ± 10	45 ± 5
t_{dif} , s	–	–	450 ± 70	600 ± 100
PSR B0950+08				
f_{dif} , kHz	1.5 ± 0.4	25 ± 10	100 ± 40	220 ± 60
t_{dif} , s	350 ± 100	400 ± 100	450 ± 120	>200

(upper graphs) and 62.43 MHz (lower graphs) obtained in individual observational sessions. Table 2 lists, together with their errors, the average values of characteristic scales of scintillations f_{dif} found from all sessions. The errors correspond to standard deviations from the mean. The slow CCF component is due to the effect of polarization. It is visible that with decreasing frequency the relative amplitude of the slow component increases; this testifies to an increase in the degree of polarization with frequency. Figure 4 presents the mean profiles of PSR B0809+74 and B0950+08 for one of the observational sessions at the low frequency 41 MHz (left-hand graphs) and mean CCF between the spectra of adjacent pulses at this frequency (right-hand graphs). The frequency resolution here was 1.25 kHz for both pulsars. To improve the signal-to-noise ratio for PSR B0950+08 observed at $f = 41 \text{ MHz}$ with the narrow-band receiver, we used a time constant of 10 ms; therefore, the components of the mean profile merge. For PSR B0809+74 a well-resolved two-peak profile with a separation between components of 96 ms is observed.

We determined the characteristic timescale of scintillations as the time shift at which the coefficient of correlation between the spectra separated by an appropriate time interval decreases by a factor of two. Figure 5 presents the corresponding functions for both pulsars obtained from observations at one

of the frequencies: 111.87 MHz for PSR B0809+74 (left) and 88.57 MHz for PSR B0950+08 (right). The average values of the characteristic scintillation scales t_{dif} found from all sessions are given together with their errors in Table 2. The errors correspond to standard deviations from the mean. For PSR B0809+74 we did not manage to determine t_{dif} at 41 and 62 MHz because of a poor signal-to-noise ratio.

4. STRUCTURAL ANALYSIS OF THE DATA

We used the obtained frequency–time correlation functions for the structural analysis of the data and, accordingly, for the study of the spectrum of ISP inhomogeneities. The power-law spectrum of electron density fluctuations is defined as

$$\Phi_{N_e}(q) = C_{N_e}^2 q^{-n}, \quad (2)$$

where $C_{N_e}^2$ characterizes the plasma turbulence level, $q = 2\pi/\rho$ and ρ are, respectively, the spatial frequency and spatial scale of an inhomogeneity in the plane perpendicular to the line of sight (generally it is a three-dimensional vector). The structure function of phase fluctuations $D(\rho)$ and spectrum Φ_{N_e} are related by the Fourier transform. In the case of a statistically uniform distribution of inhomogeneities in the medium $D(\rho)$ is described by relationship [17]

$$\begin{aligned} D_s(\rho) &= (k\Theta_0\rho)^{n-2}, & (3) \\ (k\Theta_0)^{n-2} &= A(n)(\lambda r_e)^2 C_{N_e}^2 L/(n-1), \\ A(n) &= \frac{2^{4-n}\pi^3}{[\Gamma^2(n/2)\sin(\pi n/2)]}. \end{aligned}$$

Here Θ_0 is the characteristic scattering angle, λ is the wavelength, $k = 2\pi/\lambda$ is the wavenumber, r_e is the electron classical radius, L is the effective distance to the turbulent layer or distance to the pulsar in the case of a uniform distribution of turbulence along the line of sight. The spatial scale is related to the timescale by a simple relationship $\rho = V\Delta t$, where V is the velocity of motion of the line of sight across the picture plane. If the pulsar velocity considerably exceeds the velocity of the observer and of the motion of the turbulent medium, then it determines the displacement of the line of sight. As was shown in [3], for small time shifts Δt the phase structure function $D_s(\Delta t)$ can be obtained from the correlation function of intensity fluctuations $B_I(\Delta t)$:

$$D_s(\Delta t) = \frac{B_I(0) - B_I(\Delta t)}{\langle I \rangle^2} \quad \text{at} \quad \Delta t \leq t_{\text{dif}}, \quad (4)$$

where $\langle I \rangle$ is the mean intensity for an observational session. In the frequency domain we have used the

relationship

$$D_s(\Delta f) = \frac{B_I(0) - B_I(\Delta f)}{\langle I \rangle^2} \quad \text{for} \quad \Delta f \leq f_{\text{dif}}, \quad (5)$$

where Δf is the frequency shift. To reduce the data from different frequencies to a single frequency f_0 , it is necessary to scale temporal and frequency structure functions in accordance with the law:

$$D_s(f_0, \Delta t(f_0), \Delta f(f_0)) = D_s(f, \Delta t, \Delta f)(f/f_0)^2. \quad (6)$$

As noted in [3], $\Delta t(f_0) = \Delta t(f)$; however, $\Delta f(f) \neq \Delta f(f_0)$. In the case of purely diffractive scintillations we have

$$\Delta f_d(f_0) = (f_0/f)^2 \Delta f(f). \quad (7)$$

In the presence of a strong angular refraction, i.e., when the refraction angle considerably exceeds the scattering angle, the frequency dependence Δf is quite different:

$$\Delta f_r(f_0) = (f_0/f)^3 \Delta f(f). \quad (8)$$

We have used these formulas in the analysis of our data considering two models, diffractive and refractive.

Figures 6 and 7 show for both models frequency structure functions of phase fluctuations in the double logarithmic scale for PSR B0809+74 and PSR B0950+08 respectively. All the data were reduced to the same frequency $f_0 = 1000$ MHz. As in our previous publication on the study of ISP spectra toward a number of pulsars [3–5], we have used this value of f_0 for convenience of a comprehensive analysis of all the data. In the figures the data at different frequencies are shown by different symbols. In Fig. 6 a filled circle marks a point obtained from observations at 408 MHz [18]. Statistical errors of the structure functions were estimated using equation (B12) from [19]. From Fig. 6 it is visible that for PSR B0809+74 the diffractive model (Fig. 6b) describes the experimental data much better than the refractive model (Fig. 6a). A straight line least-square-fitted to the first points of the structure functions has a slope $\beta = 1.3 \pm 0.2$. For fitting we must take the values at shifts smaller than or of the order of the characteristic frequency scale of scintillations. For PSR B0950+08 (Fig. 7) the data at different frequencies in both models differ not so strongly as for PSR B0809+74; however, the scatter of the points for the refractive model (Fig. 7a) is smaller. The largest difference takes place for a point obtained from observations at 41 MHz (filled triangle). The slope of the fitted straight line is $\beta = 0.96 \pm 0.05$.

Figures 8 and 9 show temporal structure functions of phase fluctuations for PSR B0809+74 and PSR B0950+08 respectively. In addition to our

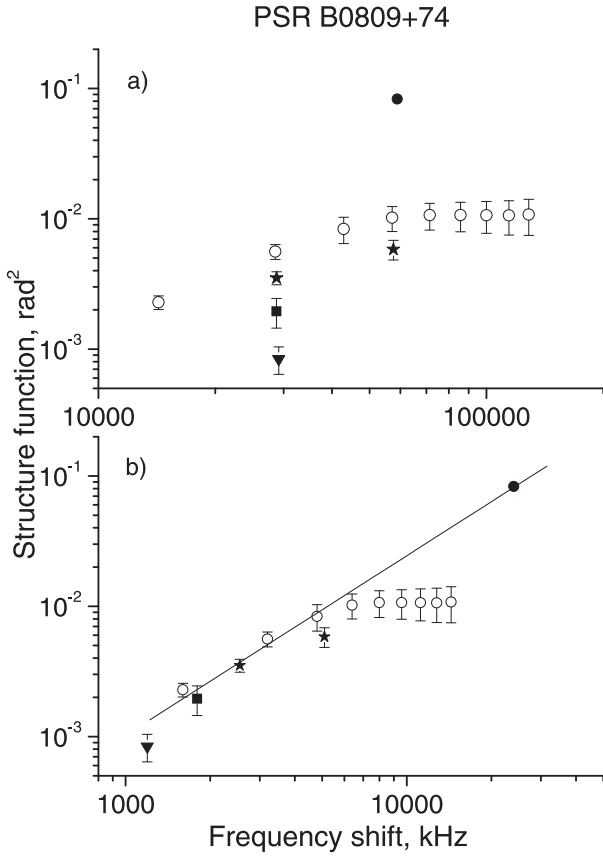


Figure 6. Frequency structure functions of phase fluctuations for PSR B0809+74 in two models: refractive (a) and diffractive (b). Open circles: 111.87-MHz data; asterisks: 88.57 MHz; square: 62.43 MHz; triangle: 41 MHz; filled circle: 408 MHz [18]. The data for all frequencies have been reduced to the same frequency $f_0 = 1000$ MHz. The straight line least-square-fitted to the first points of structure functions for the diffractive model has a slope $\beta = 1.3 \pm 0.2$.

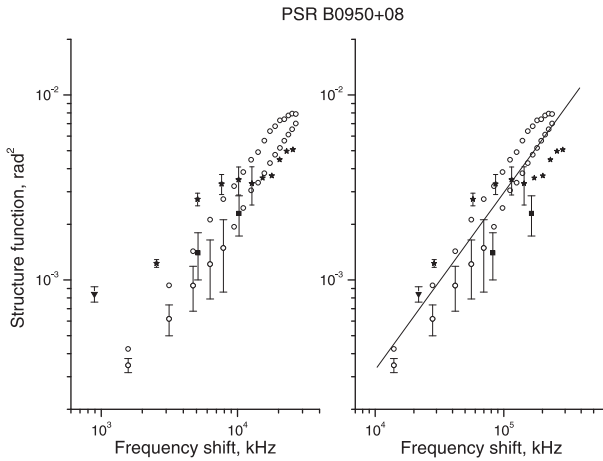


Figure 7. Same as in Fig. 6, but for PSR B0950+08. The fitted straight line has a slope $\beta = 0.96 \pm 0.05$.

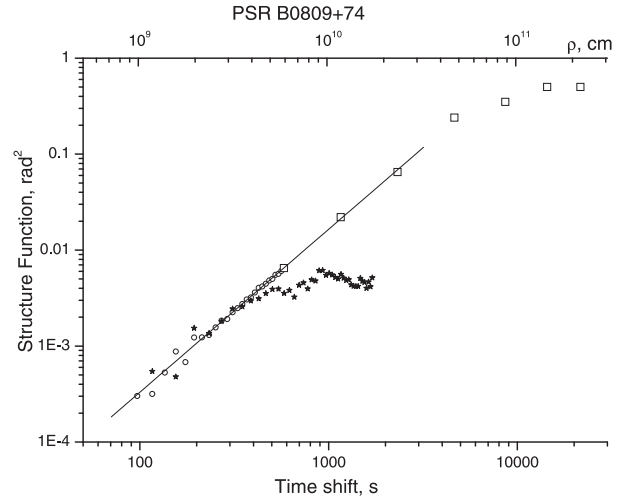


Figure 8. Temporal structure function of phase fluctuations for PSR B0809+74. Open circles: 111.87 MHz; asterisks: 88.57 MHz; small open squares: 933 MHz [19]. The data for all frequencies have been reduced to the same frequency $f_0 = 1000$ MHz. The straight line has been least-square-fitted to the initial points of the structure functions. Top: axis of the corresponding spatial scales.

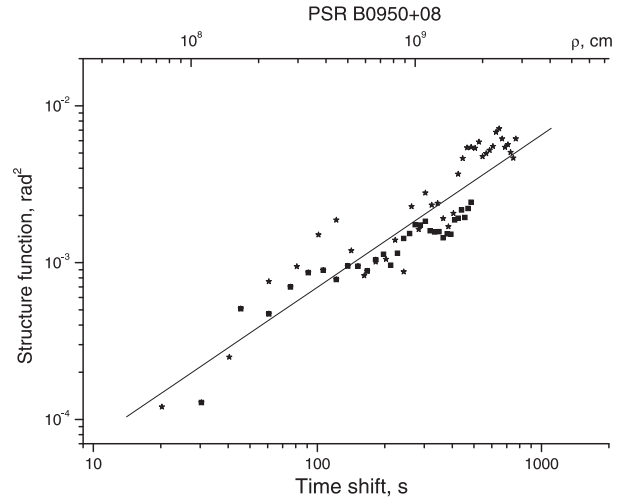


Figure 9. Temporal structure function of phase fluctuations for PSR B0950+08. Asterisks: 88.57 MHz; small filled squares: 62.43 MHz. The data for all frequencies have been reduced to the same frequency $f_0 = 1000$ MHz. The straight line has been least-square-fitted. Top: axis of the corresponding spatial scales.

data, we have used in Fig. 8 also a structure function obtained in [19] from observations at 933 MHz (open squares). It is visible that the data at different frequencies for PSR B0809+74 presented in the double logarithmic scale are well described by a unified power-law spectrum. A straight line fitted to the experimental points has a slope $\alpha = 1.7 \pm 0.04$. As it is visible from Fig. 9, for PSR B0950+08 temporal

structure functions at different frequencies reduced to 1000 MHz satisfy a power law with an exponent $\alpha = 1.0 \pm 0.05$. The scale of the upper horizontal axis in Fig. 8 and 9 corresponds to spatial scales of interstellar plasma inhomogeneities $\rho = V\Delta t$. Here we have used the pulsar velocities measured in [6]: $V = 102$ and 36.6 km/s for PSR B0809+74 and PSR B0950+08 respectively.

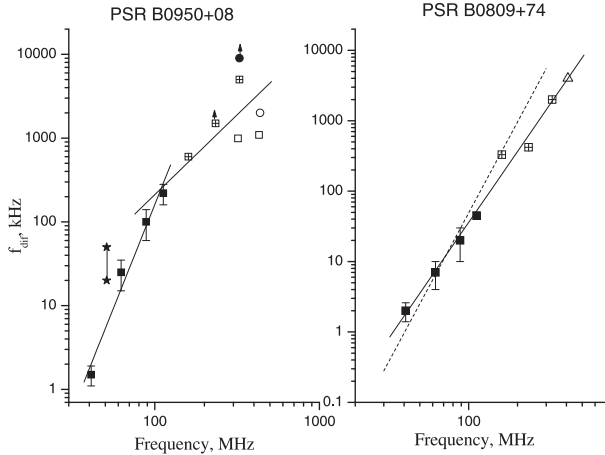


Figure 10. Characteristic frequency scale of scintillations as a function of the frequency of observation for PSR B0950+08 (left) and PSR B0809+74 (right). The filled squares show the scales obtained in this work, the asterisks the data of [20], the crust the data of [21], the open circle the data of [22], the filled circle the data of [10], the triangle the data of [18], and the open squares: data from [7]. The lines are the result of least-squares fits. The slope for PSR B0950+08 using our data is $\gamma = 4.9 \pm 0.6$, while the slope for the data at frequencies ≥ 112 MHz is $\gamma = 2 \pm 0.6$. The fitting for PSR B0809+74 fitting using all the points yielded the slope of $\gamma = 3.4 \pm 0.15$. The dashed line with a slope of 4.3 is the expected $f_{\text{dir}}(f)$ dependence.

5. DISCUSSION

As shown above, the temporal structure functions for PSR B0809+74 and PSR B0950+08 are described by a power law, and, accordingly, the spectrum of interstellar plasma inhomogeneities toward these pulsars is a power-law one with an exponent $n = \alpha + 2$; this corresponds to $n = 3.0 \pm 0.05$ for PSR B0950+08 and $n = 3.7 \pm 0.04$ for PSR B0809+74. Whereas for PSR B0809+74 the measured turbulence spectrum matches to the Kolmogorov form ($n = 3.67$), for PSR B0950+08 it is much flatter. In addition, we can say that toward PSR B0950+08 an appreciable angular refraction takes place. As shown in [3], for the diffractive model the slope of the frequency structure function is related to that of the temporal structure function as $\beta = \alpha/2$, and for the refractive model $\beta = \alpha$. For

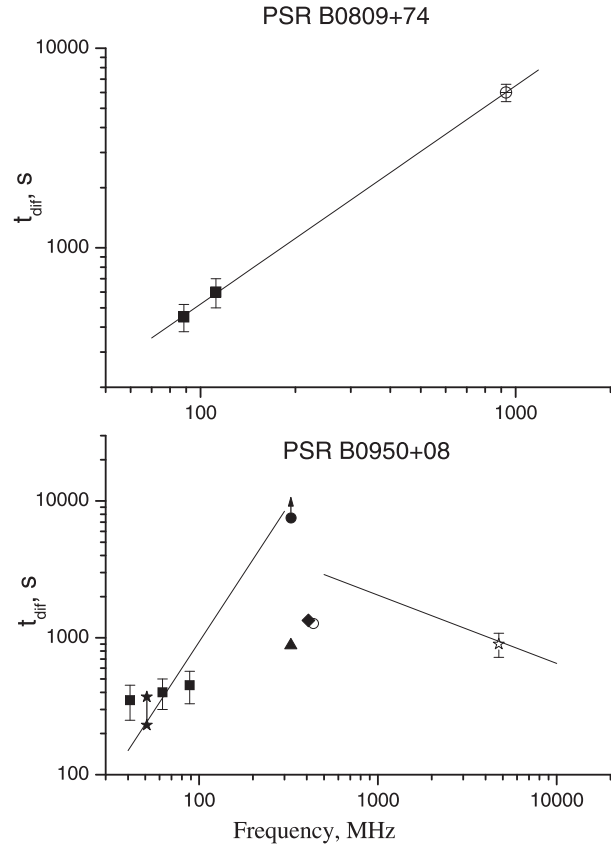


Figure 11. Characteristic temporal scale of scintillations as a function of the frequency of observation; top: PSR B0809+74, bottom: PSR B0950+08. Filled squares: scales obtained in this work, triangle: the data from [23], filled asterisks: [20], the open asterisk: [24], the diamond the data of [25], open circle: [19]. A straight line has been least-square-fitted to the data for PSR B0809+74; its slope is 1.1. Asymptotic straight lines with slopes of $\alpha = 2$ and $\alpha = -0.5$ corresponding to equations (10) and (14) are shown for PSR B0950+08.

PSR B0950+08 we have $\beta \approx \alpha$. For PSR B0809+74 the accuracy of the determination of β is low, and within the 3σ error limits the relationship $\beta = \alpha/2$ is fulfilled, though a more convincing evidence of the absence of angular refraction in this direction is a strong deviation of the data on the frequency structural function from this model (Fig. 6).

Figures 10 and 11 present the characteristic frequency and temporal scales of scintillations as functions of the frequency of observation for both pulsars. Filled squares show our measurements, other symbols denote the data taken from [7, 10, 18–25]. For the reduction of the scales f_d obtained by a different method in [21] to our measurements, we have used the relationship $f_{\text{dif}} = 0.3f_d$. We have least-square-fitted straight lines to the observation data. For PSR B0950+08 (Fig. 10) fitting

was done separately to the low-frequency data of this work (slope $\gamma = 4.9 \pm 0.6$), and to the data at frequencies $f > 112$ MHz (slope $\gamma = 2 \pm 0.6$). For PSR B0809+74 fitting for all points (Fig. 10) yields $\gamma = 3.4 \pm 0.15$. As shown above, the frequency CCF of the flux fluctuations of the pulsar PSR B0809+74 is described by the model of diffractive scintillations on inhomogeneities of the power-law spectrum of interstellar plasma turbulence with an exponent $n = 3.7$. For the diffractive model the characteristic frequency scale of scintillations is [17]

$$f_{\text{dif}} = c/(\pi R \Theta_0)^2 \propto f^{2n/(n-2)}, \quad (9)$$

where c is the velocity of light. For $n = 3.7$ the expected for PSR B0809+74 value $\gamma = 4.3$ is shown in Fig. 10 with a dotted line. This line is also consistent with the experimental points, except for the high-frequency ones. It is possible that the values of f_{dif} measured at high frequencies are underestimated because of the limited total frequency band of the observation. The characteristic timescale of the scintillations for the diffractive model is

$$t_{\text{dif}} \approx 1/k\Theta_0 V \propto f^{2/(n-2)}, \quad (10)$$

where k is the wavenumber and V is the velocity of motion of the line of sight with respect to the turbulent medium. For $n = 3.7$ the expected for PSR B0809+74 value $2/(n-2) = 1.18$; this agrees well with the experimentally obtained figure 1.1 (Fig.11). In [26] it was shown that the scintillation parameters for the pulsar PSR B0809+74 and quasar B0917+624, which is located close to the pulsar on the celestial sphere, are determined by the same turbulent medium and this medium is distributed almost uniformly on a scale of the order of 500 pc.

For the pulsar PSR B0950+08 the temporal and frequency correlation functions of the flux fluctuations are described by a more sophisticated model.

Firstly, we should take into account that the observational data correspond to two modes of scintillations. At high frequencies ($f > f_{\text{cr}}$) scintillations are weak, and at low frequencies ($f < f_{\text{cr}}$) the observation data correspond to the diffractive component of strong scintillations. Near the critical frequency f_{cr} scintillations correspond to the focusing mode, which has been poorly studied, either theoretically or experimentally. According to our data, the scintillations index is about unity at all observational frequencies; thus, scintillations are strong at frequencies $f \leq 112$ MHz. Consequently, the critical frequency $f_{\text{cr}} > 112$ MHz. According to the data [25] obtained at $f = 4.8$ GHz, scintillations of the pulsar PSR B0950+08 are weak. In the same paper an estimate of the critical frequency $f_{\text{cr}} < 700$ MHz is given. In [27] on the basis of the compilation of the observational data of 1970s an estimate of the critical frequency $f_{\text{cr}} \approx 300$ MHz is given.

Secondly, it is necessary to take into account the presence of a strong angular refraction. In this case, the characteristic frequency scale of diffractive (strong) scintillations is described by the relationship [3]

$$f_{\text{dif}} \approx c/\pi r_{\text{ef}} \Theta_0 \Theta_{\text{ref}} \propto f^{2+n/(n-2)}, \quad (11)$$

$$f < f_{\text{cr}},$$

where r_{ef} is the effective distance to the turbulent layer, Θ_{ref} is the characteristic angle of refraction, Θ_0 is the characteristic scattering angle determined by (3). For $n = 3$ equation (11) yields $f_{\text{dif}} \propto f^5$. The observational data indeed correspond to a power law with a turnover. At low frequencies ($f \leq 112$ MHz) the exponent $\gamma = 4.9 \pm 0.6$; this is consistent with the expected value for the mode of strong scintillations in the presence of refraction. Therefore, we can assert that the critical frequency $f_{\text{cr}} > 112$ MHz. In the case of weak scintillations we should replace the scattering angle Θ_0 with the Fresnel angle

$$\Theta_{\text{Fr}} = (1/kr_{\text{ef}})^{1/2}. \quad (12)$$

As a result we obtain

$$f_{\text{dif}} \approx c/\pi r_{\text{ef}} \Theta_{\text{Fr}} \Theta_{\text{ref}} \propto f^{2.5}. \quad (13)$$

At high frequencies $f \geq 112$ MHz the exponent $\gamma = 2 \pm 0.6$; this also agrees with the expected value for the mode of weak scintillations.

The characteristic timescale of scintillations for PSR B0950+08 is also described by a power law with a turnover. At low frequencies scintillations are strong, and the characteristic timescale of scintillations is determined by formula (10). At high frequencies scintillations are weak, and the characteristic timescale of scintillations is

$$t_{\text{dif}} \approx (r_{\text{ef}}/k)^{1/2}/V_{\text{ef}} \propto f^{-1/2}, \quad (14)$$

where V_{ef} is the velocity of motion of the line of sight with respect to the turbulent layer. The asymptotic relationships (10) and (14) are shown in Fig. 11 with straight lines. We see that the theoretical dependences agree well enough with the experimental points. From the timescale of weak scintillations we can determine the distance to the layer responsible for the radiowave modulation. If L is the distance from the observer to the turbulent layer and R is the distance from the observer to the pulsar, the effective distance is

$$1/r_{\text{ef}} = 1/(R-L) + 1/L. \quad (15)$$

The effective velocity is

$$V_{\text{ef}} = V_o(R-L)/R + V_p L/R, \quad (16)$$

where V_o and V_p are the components of the velocities of the observer and pulsar in the picture plane respectively. The pulsar velocity is $V_p = 36.6$ km/s [6];

therefore, $V_p \cong V_0$, and $V_{\text{ef}} \cong V_p \cong 30$ km/s. Using this value of V_{ef} in (14) and supposing $t_0 = 15$ min at the frequency $f = 4.8$ GHz [25], we obtain

$$L(R - L)/R \cong 9.7 \text{ pc.} \quad (17)$$

For this equation we find the solutions $L_1 = 10$ pc and $L_2 = 252$ pc. Therefore, the turbulent layer is either near the observer or near the pulsar. It should be noted that parameters of the scintillations of the pulsar PSR B0950+08 are rather close to those of the pulsar B0437-47 [5], which is located at approximately the same galactic longitude. For the latter pulsar it was shown in [5] that its scintillations as well as those of the quasar PKS 0405-385, at a small angular distance, are determined by a layer of the medium with enhanced turbulence at 10 pc from the observer. Therefore, we can accept that the pulsar PSR B0950+08 scintillates on the same layer of the turbulent medium and that the right solution is $L_1 = 10$ pc.

Table 3. Local turbulence levels

PSR	$D_s(\rho_0)$, rad ²	L , pc	$D_s(\rho_0)/L$, rad ² /pc	ΔN_e , cm ⁻³
B0329+54	0.034	1000	3×10^{-5}	7.7×10^{-4}
B0437-47	0.0033	10	3×10^{-4}	2.4×10^{-3}
B0809+74	0.0003	433	1×10^{-6}	1.4×10^{-4}
B0950+08	0.002	10	2×10^{-4}	2×10^{-3}

Let us estimate the turbulence level toward PSR B0809+74 and PSR B0950+08. Note that we cannot use for the comparative analysis the values of $C_{N_e}^2$, because they change their dimension with changing spectrum exponent n . We will use the values of the structure function on a selected scale $\rho_0 = 10^7$ m at a frequency $f = 1$ GHz. The local level of turbulence is related to the gradient $D_s(\rho_0)$ as follows: $(d/L)D_s(\rho_0) \approx D_s(\rho_0)/L$, where L is the characteristic thickness of the layer of the medium. The value of $D_s(\rho_0)/L$ is proportional to the mean square of electron density fluctuations on inhomogeneities with a characteristic scale ρ_0 ; for $\rho_0 = 10^7$ m we have:

$$\begin{aligned} & D_s(\rho_0)/L \text{ [rad}^2/\text{pc]} \\ & \cong 50 \langle [\Delta N_e(\rho_0)]^2 \rangle \text{ [cm}^{-6}\text{]}. \end{aligned} \quad (18)$$

Table 3 lists the values of $D_s(\rho_0)$ at a frequency $f = 1$ GHz together with the values of $D_s(\rho_0)/L$ and ΔN_e for the pulsars studied by us in [3, 5] and in this paper. The distribution of the estimated local turbulence levels corresponds to three components of the interstellar medium mentioned in the Introduction. The greatest values of ΔN_e correspond to the layer with an enhanced turbulence level (layer C): the pulsars PSR B0437-47 and PSR B0950+08 scintillate on its inhomogeneities. The minimum value of ΔN_e

obtained toward the pulsar PSR B0809+74 corresponds to a cavern. The intermediate value of ΔN_e is obtained toward the pulsar PSR B0329+54; it corresponds to turbulent plasma in the space between spiral arms (component A).

6. CONCLUSION

As a result of the analysis of the phase structure functions obtained by us from the study of interstellar scintillations toward PSR B0809+74 and PSR B0950+08 at low frequencies 41-112 MHz with invoking the previously published higher frequency data, we have shown that the spectrum of interstellar plasma inhomogeneities toward both pulsars is described by a power law. The spectrum exponent toward PSR B0950+08 differs appreciably from the Kolmogorov exponent; it is $n = 3.00 \pm 0.05$. Toward PSR B0809+74 the spectrum is a power law with an exponent $n = 3.7 \pm 0.1$; within the error limits this correspond to the Kolmogorov spectrum. The analysis of the frequency dependence of the diffraction parameters has shown that toward PSR B0950+08 the transition to the weak scintillation mode takes place approximately at a frequency of 200-300 MHz; here is a turnover in relationships $t_{\text{dif}}(f)$ and $f_{\text{dif}}(f)$. The experimental data match well enough the dependence expected by the theory.

As a result of the analysis of the temporal and frequency phase structural functions for a purely diffractive model and model with a strong angular refraction, we have shown that toward PSR B0950+08 there exists a strong angular refraction. The conducted analysis of scintillations of this pulsar at different frequencies has shown that the distribution of inhomogeneities along the line of sight is not uniform and that the scintillations of PSR B0950+08 take place on a turbulent layer with enhanced electron density (layer C), which is located at a distance of about 10 pc from the observer. The same layer is responsible for the scintillations of PSR B0437-47 and and of the quasar PKS 0405-385. Here the local turbulence level on a scale $\rho_0 = 10^7$ m is 20 times higher than in the extended region with a size of the order of 430 pc responsible for the scintillations of PSR B0809+74.

ACKNOWLEDGMENTS

This work was supported by the Russian Foundation for Basic Research (project codes 06-02-16810 and 06-02-16888) and by the Program of Basic Research of the Presidium of the Russian Academy of Sciences "Origin and evolution of stars and galaxies".

-
1. J. W. Armstrong, B. J. Rickett, and S. R. Spangler, *Astrophys. J.* **443**, 209 (1995).
 2. V. I. Shishov and T. V. Smirnova, *Astron. Zh.* **79**, 810 (2002) [*Astron Rep.* **46**, 731 (2002)].
 3. V. I. Shishov, T. V. Smirnova, W. Sieber, *et al.*, *Astron. and Astrophys.* **404**, 557 (2003).
 4. T. V. Smirnova, V. I. Shishov, W. Sieber, *et al.*, *Astron. and Astrophys.* **455**, 195 (2006).
 5. T. V. Smirnova, C. R. Gwinn, and V. I. Shishov, *Astron. and Astrophys.* **453**, 453 (2006).
 6. W. E. Brisken, J. M. Benson, W. M. Goss, and S. E. Thorsett, *Astrophys. J. (Letters)* **573**, 111 (2002).
 7. J. M. Cordes, J. M. Weisberg, and V. Boriakoff, *Astrophys. J.* **288**, 221 (1985).
 8. A. V. Pynzar' and V. I. Shishov, *Astron. Zh.* **74**, 663 (1997) [*Astron Rep.* **41**, 586 (1997)].
 9. S. L. Snowden, D. P. Cox, D. McCammon, and W. T. Sanders, *Astrophys. J.* **354**, 211 (1990).
 10. N. D. Bhat, Y. Gupta, and A. Pramesh Rao, *Astrophys. J.* **500**, 262 (1998).
 11. J. Demmett-Thorpe and A. G. de Bruyn, *Astrophys. and Space Sci.* **278**, 101 (2001).
 12. B. J. Rickett, L. Kedziora-Chudczer, and D. L. Jauncey, *Astrophys. J.* **581**, 103 (2002).
 13. J. M. Rankin, R. Ramachandran, and S. A. Suleymanova, *Astron. and Astrophys.* **429**, 999 (2005).
 14. T. V. Shabanova and Yu. P. Shitov, *Astron. and Astrophys.* **418**, 203 (2004).
 15. J. H. Taylor, R. N. Manchester, and A. G. Lyne, *Astrophys. J.* **88**, 529 (1993).
 16. S. Johnston, G. Hobbs, S. Vigeland, *et al.*, *Monthly Not. Roy. Astron. Soc.* **364**, 1397 (2005).
 17. T. V. Smirnova, V. I. Shishov and D. R. Stinebring, *Astron. Zh.* **75**, 866 (1998) [*Astron Rep.* **42**, 766 (1998)].
 18. F. G. Smith, N. C. Wright, *Monthly Not. Roy. Astron. Soc.* **214**, 97 (1985).
 19. B. J. Rickett, Wm. A. Coles, and J. Markkanen, *Astrophys. J.* **533**, 304 (2000).
 20. J. A. Phillips and A. W. Clegg, *Nature* **360**, 137 (1992).
 21. G. R. Huguenin, J. H. Taylor, and M. Jura, *Astrophys. J. (Letters)* **4**, 71 (1969).
 22. S. Johnston, L. Nicastro, and B. Koribalski, *Monthly Not. Roy. Astron. Soc.* **297**, 108 (1998).
 23. F. G. Smith and N. C. Wright, *Monthly Not. Roy. Astron. Soc.* **214**, 97 (1985).
 24. V. Balasubramanian and S. Krishnamohan, *Astron. and Astrophys.* **6**, 35 (1985).
 25. V. M. Malofeev, V. I. Shishov, W. Sieber, *et al.*, *Astron. and Astrophys.* **308**, 180 (1996).
 26. V. I. Shishov, T. V. Smirnova and S. A. Tul'bashev, *Astron. Zh.* **82**, 281 (2005) [*Astron Rep.* **49**, 250 (2005)].
 27. A. V. Pynzar' and V. I. Shishov, *Astron. Zh.* **57**, 1187 (1980) [*Sov. Astron.* **24**, 685 (1980)].